Combination of D* Differential Cross Section Measurements in Deep-Inelastic ep Scattering at HERA

H1 and ZEUS Collaborations

Abstract

H1 and ZEUS have recently published differential cross sections for D* production from their respective final data sets, in a very similar phase space. These cross sections are combined at the visible cross section level, taking into account all relevant correlations, thereby significantly reducing the uncertainties. NLO QCD predictions are compared to the results.

1 Introduction

Measurements of open charm production in deep-inelastic electron[1]-proton scattering (DIS) at HERA provide important input for stringent tests of the theory of strong interactions, quantum chromodynamics (QCD).

H1 [1, 2] and ZEUS [3] have recently published measurements of differential cross sections for D^* production from the final HERA II sets, in a similar limited phase space. This also includes extrapolations to the full phase space, i.e. the charm contributions to the proton structure functions, which have partially already been combined [4] with measurements from other charm production processes [5–20] and used to measure the charm quark mass and to improve predictions for W and Z production at LHC [4].

This note addresses the combination of cross sections for D^* [1–3] at visible level, such that one consistent data set is obtained, which can be compared directly to differential NLO cross section predictions without the need for extrapolation. The combination is based on the procedure described in [21–23], including a full treatment of the correlated uncertainties, similar to the one used for the combinations at structure function level [4]. This yields a significant reduction of the overall uncertainty of the measurements.

In general, the analysis of fully reconstructed D^* mesons yields the best signal-to-background ratio for charm production. However, the branching ratios are small and the phase space of charm production accessible with D^* mesons is restricted because all products from the D^* meson decay have to be measured. For the details of the experimental analysis, the reader is referred to the previous work [1–3].

Combinations are made for the cross sections in terms of the virtuality, Q^2, of the exchanged photon, the inelasticity y, the transverse momenta, $p_T^{D^*}$, and pseudorapidities, η^{D^*}, of the outgoing D^* mesons, and the fragmentation variable $z^{D^*} = (E^{D^*} - p_Z^{D^*})/(2E_e y)$, where E_e is the incoming electron energy. The double differential cross sections in Q^2 and y are also combined.

The massive fixed-flavour-number-scheme (FFNS) is used for theory predictions throughout this note, since it is the only scheme for which fully differential calculations [24] are available at next-to-leading order (NLO).

2 Combination of H1 and ZEUS measurements

2.1 Theoretical predictions

QCD predictions from charm production for all distributions were obtained at next-to-leading order in QCD ($O(\alpha_s)^2$) using HVQDIS [24] in the 3-flavour FFNS scheme.

The following parameters are used in the calculations and the corresponding variations are used to estimate the associated uncertainties

- **pole mass of the charm quark** $m_c = 1.5 \pm 0.15$ GeV;

---

[1]In this note 'electron' is used to denote both electron and positron if not otherwise stated.

- **renormalisation and factorisation scales** $\mu_f = \mu_r = \sqrt{Q^2 + 4m_c^2}$, varied simultaneously up or down by a factor of two for the extrapolation from $Q^2 < 100$ GeV^2 to $Q^2 < 1000$ GeV^2, for which only the shape was relevant, and varied independently by the same factor for the absolute predictions, with the restriction that the difference between the two scales never exceeds a factor 2.

- **strong coupling constant** $\alpha_s^{n_f=3}(M_Z) = 0.105 \pm 0.002$, corresponding to $\alpha_s^{n_f=5}(M_Z) = 0.116 \pm 0.002$;

- **the proton structure** is described by a series of FFNS variants of the HERAPDF1.0 set [23] at NLO, evaluated for $m_c = 1.5 \pm 0.15$ GeV, for $\alpha_s^{n_f=3}(M_Z) = 0.105 \pm 0.002$, and for different scales. Charm data are not included in these fits. The effects of the PDF uncertainties are calculated according to the HERAPDF1.0 prescription [23].

- **charm fragmentation** is treated as detailed in [4].

The small beauty contribution needs a detailed treatment of b hadron to D^* decays and is therefore obtained from the RAPGAP [25] MC, renormalized to independent measurements as detailed in [2, 3]. The sum of the HVQDIS charm and scaled RAPGAP beauty predictions will be referred to as NLO predictions in the following.

2.2   Combination method

Both measurements to be combined are already corrected to Born level (using running α) and include both the charm and beauty contributions to D^* production. The total expected beauty contribution is small ($\sim 3\%$). The overall phase space for the combined cross sections is given by

- $5 < Q^2 < 1000$ GeV^2,

- $0.02 < y < 0.7$,

- $1.5 < P_T^{D^*} < 20$ GeV,

- $|\eta^{D^*}| < 1.5$.

In order to make the input data sets compatible to this phase space and with each other, some small modifications are applied before the combination. From the two sets of measurements in [2], the one compatible with the cuts on $p_T^{D^*}$ and η^{D^*} quoted above is chosen. Since this measurement extends only up to $Q^2 < 100$ GeV^2 it was extrapolated to $Q^2 < 1000$ GeV^2 using the shape of the HVQDIS [24] prediction, normalized to the measurement of the cross section between 100 and 1000 GeV^2 taken from [1]. In order to cope with some differences in the binning for the Q^2 distribution between [3] and [1, 2], the first two Q^2 bins from [2] were combined, and the highest Q^2 bins from [3] and [1] were obtained from an integral of the double differential cross sections, which have a common binning. For the data from [2], the D^* branching ratio was updated to the latest PDG value [26].

The combination of the data sets uses the χ^2 minimisation method developed for the combination of inclusive DIS cross sections [21, 23], as implemented in HERAverager [27]. The

χ^2 function is defined as described in [4] and takes into account the correlated systematic uncertainties for the H1 and ZEUS cross section measurements. The statistical uncertainaties are treated as uncorrelated, while most of the systematic uncertainties are treated as point-to-point correlated. Asymmetric systematic uncertainties are symmetrised before performing the combination. Except for the branching ratio uncertainty, which is treated as correlated, all systematic uncertainties are treated as independent between H1 and ZEUS. Each combined point consists of the combination of exactly two measurements.

Since the data are statistically correlated between the different distributions, each distribution was combined separately. The individual data sets as well as the results of the combination are shown in Figs. 1 to 6. The combinations in the different variables have a χ^2 probability varying between 15% and 86%, i.e. the two data sets are consistent.

3 Combined D* Cross Sections

The combined cross sections as a function of Q^2, y, p_T, η and z, and the double differential cross sections in Q^2 and y are shown in Figs. 7 to 12 and compared to NLO predictions.

In general the predictions describe the data very well. The data reach a precision of about 5% over a large fraction of the measurede phase space, while the typical theory uncertainty ranges from 30% at low Q^2 to 10% at high Q^2. NNLO calculations would therefore be very helpful to match the data precision.

Both in the single differential and in the double differential distributions the central theory prediction shows a somewhat softer y distribution than the data. The central prediction for z^{D^*} is a bit wider than the measured distribution.

4 Conclusions

Measurements of D* production in deep-inelastic ep scattering by the H1 and ZEUS experiments are combined at the vsisble cross section level, accounting for the systematic correlations. The data sets were found to be consistent, and the combined sets exhibits significantly reduced uncertainties. The combined data are compared to NLO QCD predictions. The predictions describe the data very well, but also give some hints for possible future improvements.

Acknowledgements

References

[1] F. D. Aaron *et al.* [H1 Collaboration], Phys. Lett. **B686**, (2010) 91 [arXiv:0911.3989].

[2] F. D. Aaron *et al.* [H1 Collaboration], Eur. Phys. J. **C71**, (2011) 1769 [arXiv:1106.1028].

[3] H. Abramowicz *et al.* [ZEUS Collaboration], DESY-13-054, accepted by JHEP .

[4] F.D. Aaron *et al.* [H1 and ZEUS Collaborations], Eur. Phys. J. **C73** (2013) 2311 [arXiv:1106.1028].

[5] C. Adloff *et al.* [H1 Collaboration], Z.Phys **C72**, (1996) 593 [hep-ex/9607012].

[6] J. Breitweg *et al.* [ZEUS Collaboration], Phys. Lett. **B407**, (1997) 402 [hep-ex/9706009].

[7] C. Adloff *et al.* [H1 Collaboration], Nucl. Phys. **B545**, (1999) 21 [hep-ex/9812023].

[8] J. Breitweg *et al.* [ZEUS Collaboration], Eur. Phys. J. **C12**, (2000) 35 [hep-ex/9908012].

[9] C. Adloff *et al.* [H1 Collaboration], Phys. Lett. **B528**, (2002) 199 [hep-ex/0108039].

[10] S. Chekanov *et al.* [ZEUS Collaboration], Phys. Rev. **D69**, (2004) 012004 [hep-ex/0308068].

[11] A. Aktas *et al.* [H1 Collaboration], Eur. Phys. J. **C38**, (2005) 447 [hep-ex/0408149].

[12] A. Aktas *et al.* [H1 Collaboration], Eur. Phys. J. **C40**, (2005) 349 [hep-ex/0411046].

[13] A. Aktas *et al.* [H1 Collaboration], Eur. Phys. J. **C45**, (2006) 23 [hep-ex/0507081].

[14] A. Aktas *et al.* [H1 Collaboration], Eur. Phys. J. **C51**, (2007) 271 [hep-ex/0701023].

[15] S. Chekanov *et al.* [ZEUS Collaboration], JHEP **0707**, (2007) 074 [arXiv:0704.3562].

[16] S. Chekanov *et al.* [ZEUS Collaboration], Eur. Phys. J. **C63**, (2009) 171 [arXiv:0812.3775].

[17] S. Chekanov *et al.* [ZEUS Collaboration], Eur. Phys. J. **C65**, (2010) 65 [arXiv:0904.3487].

[18] F. D. Aaron *et al.* [H1 Collaboration], Eur. Phys. J. **C65**, (2010) 89 [arXiv:0907.2643].

[19] H. Abramowicz *et al.* [ZEUS Collaboration], JHEP **1011**, (2010) 009 [arXiv:1007.1945].

[20] F. D. Aaron *et al.* [H1 Collaboration], Eur. Phys. J. **C71**, (2011) 1509 [arXiv:1008.1731].

[21] A. Glazov, AIP Conf. Proc. **792**, (2005) 237.

[22] A. Atkas *et al.* [H1 Collaboration], Eur. Phys. J. **C63**, (2009) 625 [arXiv:0904.0929].

[23] F. D. Aaron *et al.* [H1 and ZEUS Collaboration], JHEP **1001**, (2010) 109 [arXiv:0911.0884].

[24] B. W. Harris and J. Smith, Phys. Rev. **D57**, (1998) 2806 [hep-ph/9706334].

[25] H. Jung, Comp. Phys. Comm. **86** (1995) 147.

[26] J. Beringer *et al.* [Particle Data Group], Phys. Rev. **D86** (2012) 1.
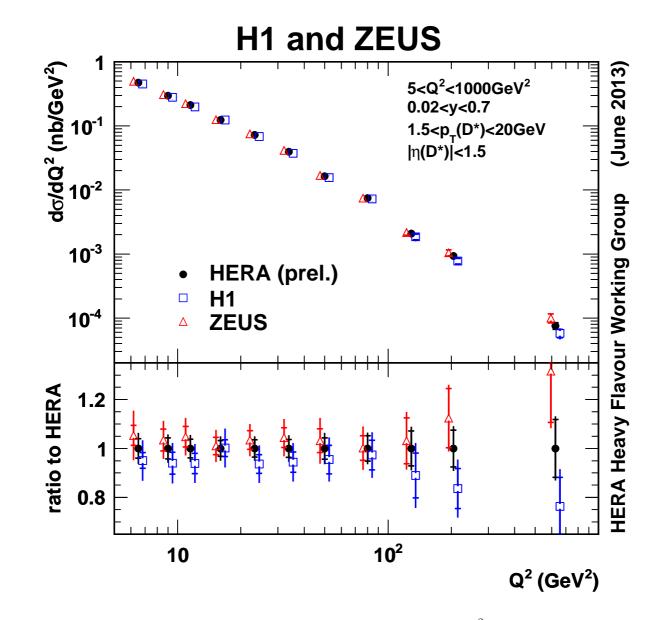
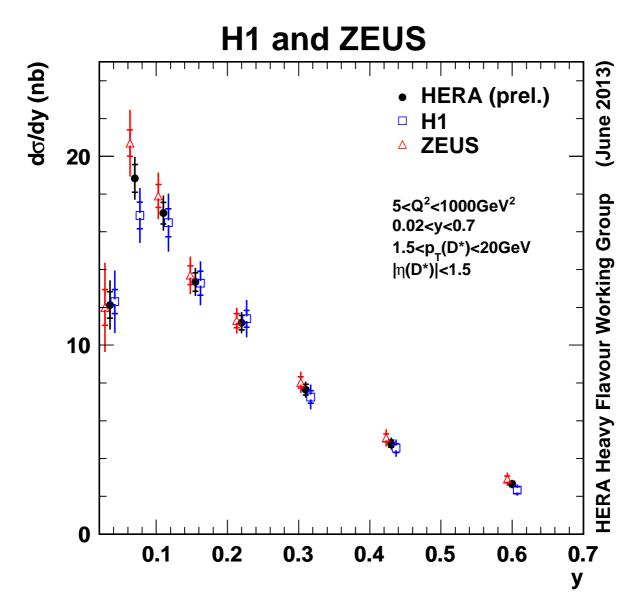[27] https://wiki-zeuthen.desy.de/HERAverager/

Figure 1: Differential D^* production cross section as a function of Q^2. The triangles and open squares are the cross sections before combination, shown with a small horizontal offset for better visibility. The filled points are the combined cross sections. The inner error bars indicate the statistical uncertainties before combination, and the uncorrelated part of the uncertainties after combination. The outer error bars represent the total uncertainties. The bottom part shows the ratio of these cross sections with respect to the central value of the combined cross sections.

Figure 2: Differential D^* production cross section as a function of y. The triangles and open squares are the cross sections before combination, shown with a small horizontal offset for better visibility. The filled points are the combined cross sections. The inner error bars indicate the statistical uncertainties before combination, and the uncorrelated part of the uncertainties after combination. The outer error bars represent the total uncertainties.
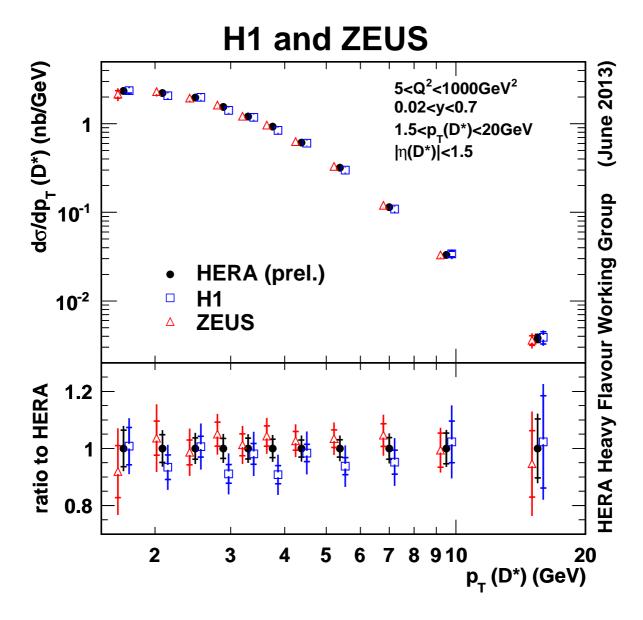
H1 and ZEUS

Figure 3: Differential cross section as a function of p_T. The triangles and open squares are the cross sections before combination, shown with a small horizontal offset for better visibility. The filled points are the combined cross sections. The inner error bars indicate the statistical uncertainties before combination, and the uncorrelated part of the uncertainties after combination. The outer error bars represent the total uncertainties. The bottom part shows the ratio of these cross sections with respect to the central value of the combined cross sections.
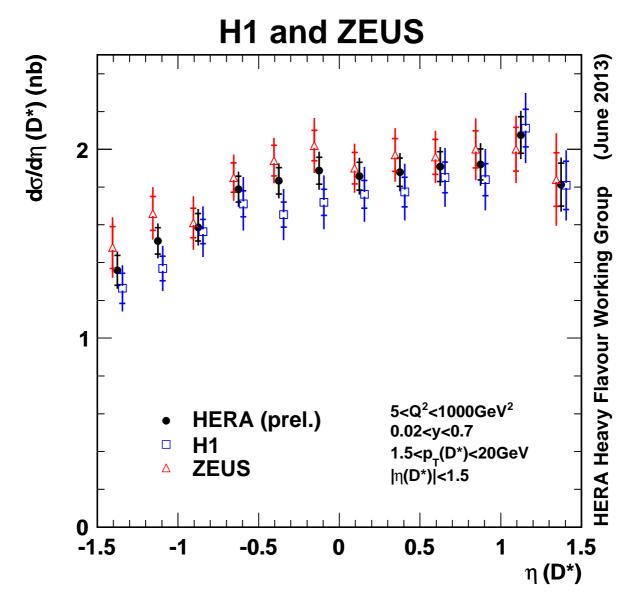
Figure 4: Differential D^* production cross section as a function of η. The triangles and open squares are the cross sections before combination, shown with a small horizontal offset for better visibility. The filled points are the combined cross sections. The inner error bars indicate the statistical uncertainties before combination, and the uncorrelated part of the uncertainties after combination. The outer error bars represent the total uncertainties.
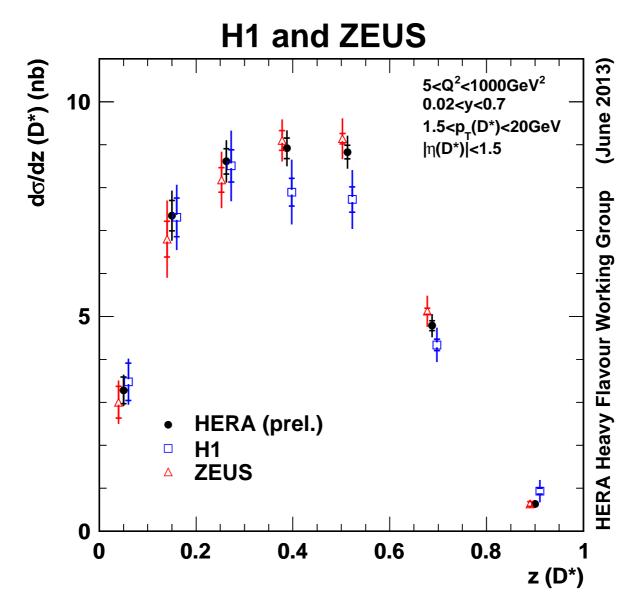
Figure 5: Differential D^* production cross section as a function of z. The triangles and open squares are the cross sections before combination, shown with a small horizontal offset for better visibility. The filled diamonds are the combined cross sections. The inner error bars indicate the statistical uncertainties before combination, and the uncorrelated part of the uncertainties after combination. The outer error bars represent the total uncertainties.
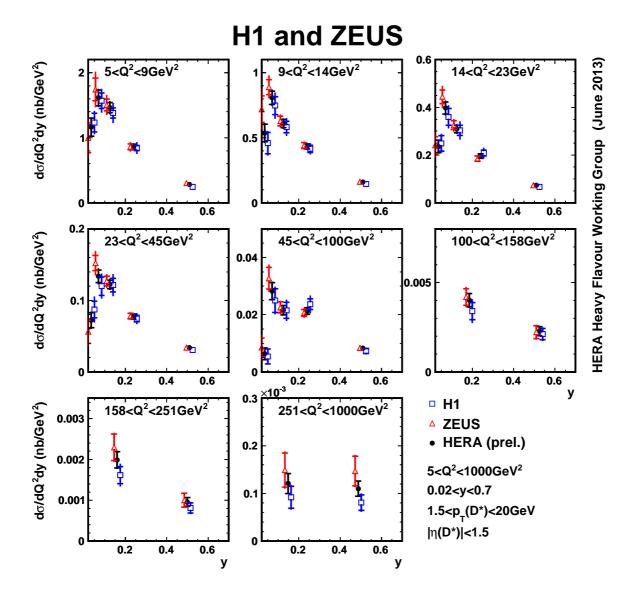
H1 and ZEUS

5<Q²<9GeV²

9<Q²<14GeV²

14<Q²<23GeV²

23<Q²<45GeV²

45<Q²<100GeV²

100<Q²<158GeV²

158<Q²<251GeV²

251<Q²<1000GeV²

dσ/dQ²dy (nb/GeV²)

y

×10⁻³

HERA Heavy Flavour Working Group (June 2013)

□ H1
△ ZEUS
● HERA (prel.)

5<Q²<1000GeV²
0.02<y<0.7
1.5<p$_T$(D*)<20GeV
|η(D*)|<1.5

Figure 6: Double differential D^* production cross sections as a function of Q^2 and y. The triangles and open squares are the cross sections before combination, shown with a small horizontal offset for better visibility. The filled points are the combined cross sections. The inner error bars indicate the statistical uncertainties before combination, and the uncorrelated part of the uncertainties after combination. The outer error bars represent the total uncertainties.
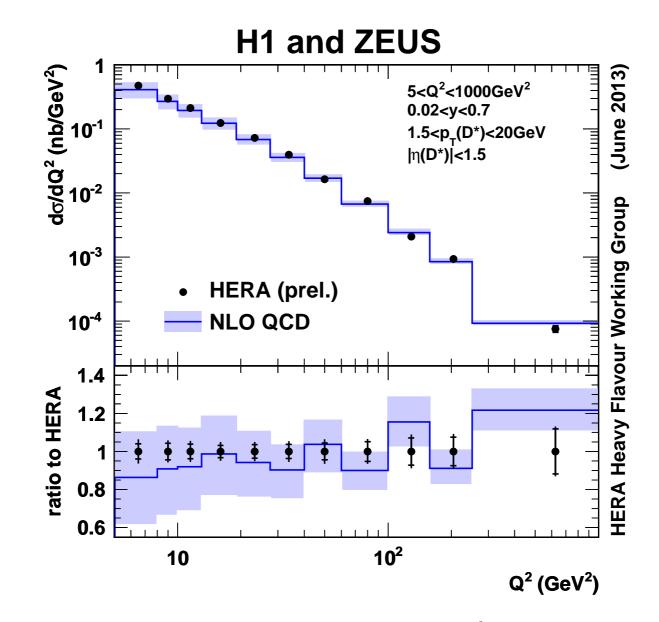
Figure 7: Differential D^* production cross section as a function of Q^2. The data points are the combined cross sections. The inner error bars indicate the uncorrelated part of the uncertainties. The outer error bars represent the total uncertainties. Also shown are the NLO predictions from HVQDIS (including the beauty contribution as obtained from RAPGAP, normalized to independent data sets), and their uncertainty band. The bottom part shows the ratio of these cross sections with respect to the central value of the combined cross sections.
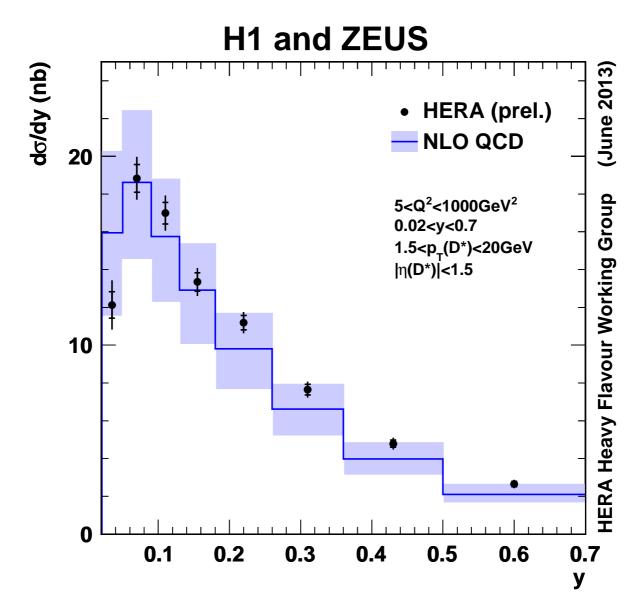
H1 and ZEUS

Figure 8: Differential D^* production cross section as a function of y. The data points are the combined cross sections. The inner error bars indicate the uncorrelated part of the uncertainties. The outer error bars represent the total uncertainties. Also shown are the NLO predictions from HVQDIS (including the beauty contribution as obtained from RAPGAP, normalized to independent data sets), and their uncertainty band.
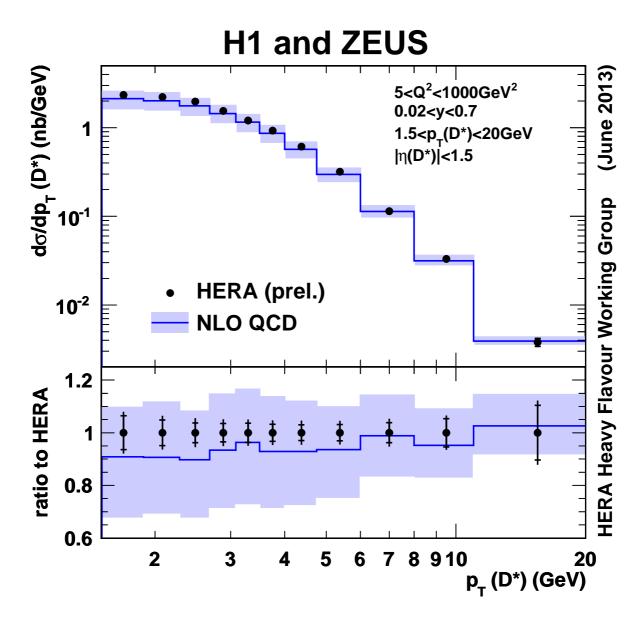
Figure 9: Differential D^* production cross section as a function of p_T. The data points are the combined cross sections. The inner error bars indicate the uncorrelated part of the uncertainties. The outer error bars represent the total uncertainties. Also shown are the NLO predictions from HVQDIS (including the beauty contribution as obtained from RAPGAP, normalized to independent data sets), and their uncertainty band. The bottom part shows the ratio of these cross sections with respect to the central value of the combined cross sections.
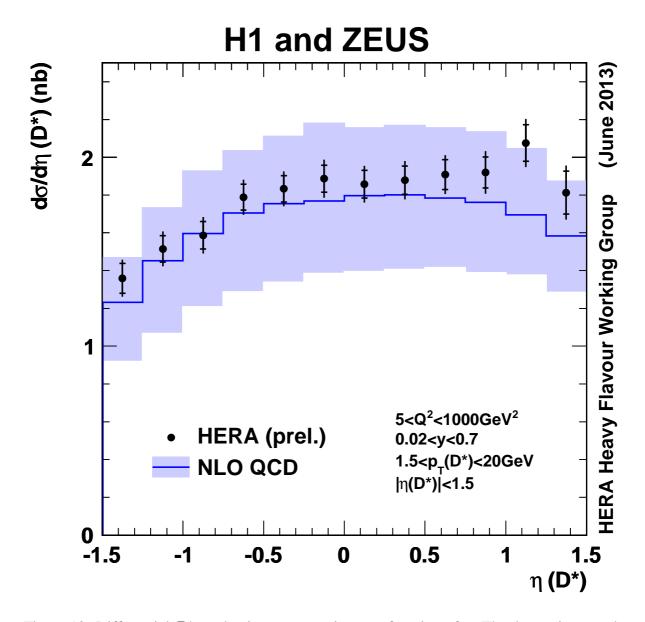
Figure 10: Differential D^* production cross section as a function of η. The data points are the combined cross sections. The inner error bars indicate the uncorrelated part of the uncertainties. The outer error bars represent the total uncertainties. Also shown are the NLO predictions from HVQDIS (including the beauty contribution as obtained from RAPGAP, normalized to independent data sets), and their uncertainty band.
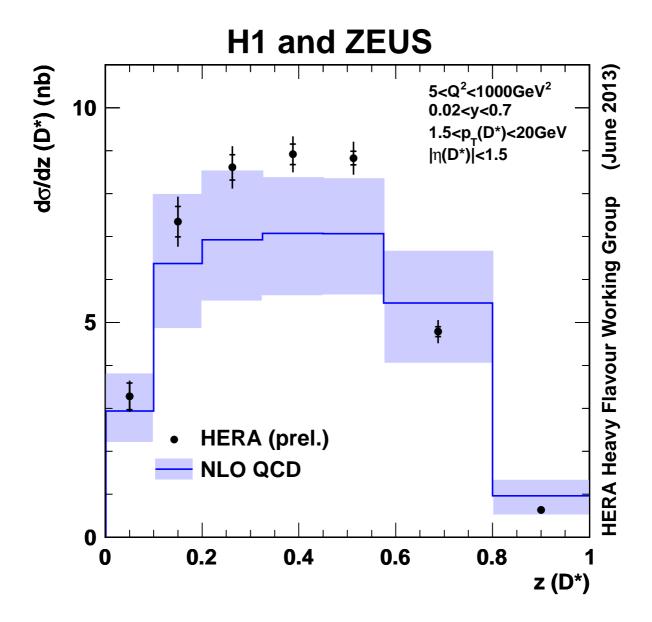
Figure 11: Differential D^* production cross section as a function of z. The data points are the combined cross sections. The inner error bars indicate the uncorrelated part of the uncertainties. The outer error bars represent the total uncertainties. Also shown are the NLO predictions from HVQDIS (including the beauty contribution as obtained from RAPGAP, normalized to independent data sets), and their uncertainty band.
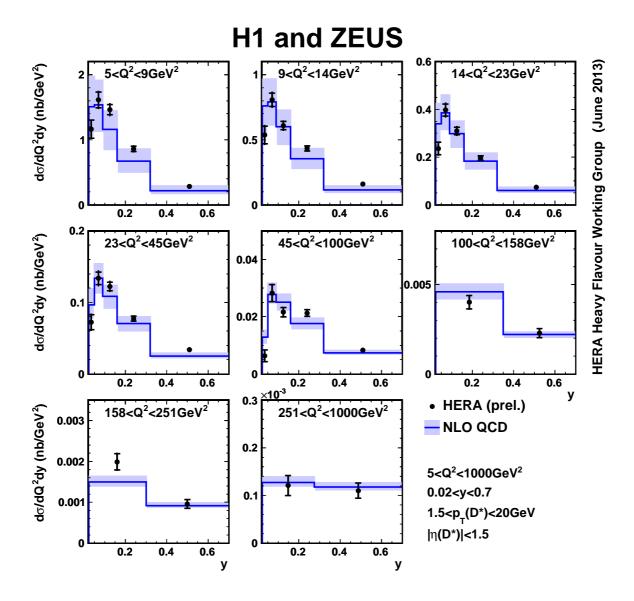
H1 and ZEUS

Figure 12: Double differential D^* production cross section as a function of Q^2 and y. The data points are the combined cross sections. The inner error bars indicate the uncorrelated part of the uncertainties. The outer error bars represent the total uncertainties. Also shown are the NLO predictions from HVQDIS (including the beauty contribution as obtained from RAPGAP, normalized to independent data sets), and their uncertainty band.